RESEARCH ARTICLE　　　　　　　　　　　　　　　　　　　　　　　**OPEN ACCESS**

IN-VITRO EVALUATION OF Zn-42Mg-4Ca ALLOY FABRICATED BY POWDER METALLURGY AS A BIODEGRADABLE BIOMATERIAL

Jorge Alberto Carvalho*[1,2], Márcio T. Fernandes[2], Alexandre A. Ribeiro[3] and José Adilson Castro[2]

[1]Coordenação de Engenharia Mecânica, Centro Federal de Educação Tecnológica-Celso Suckow da Fonseca, Angra dos Reis (RJ), Brazil; [2]Programa de Pós-graduação em Engenharia Metalúrgica, Universidade Federal Fluminense, Volta Redonda (RJ), Brazil; [3]Divisão de Materiais – Instituto Nacional de Tecnologia, Rio de Janeiro (RJ), Brazil

ARTICLE INFO

ABSTRACT

In this study, a biodegradable alloy Zn-42Mg-4Ca alloy fabricated by powder metallurgy was evaluated. The idea was to create an alloy that could optimize the good behaviors of some recognized biocompatible elements as zinc, magnesium, and calcium. The alloy's corrosion resistancewas investigated, evaluating its biodegradation behavior in a simulated physiological environment and the potential-dynamic polarization curve. Additionally, microhardness analyses were carried out as a mechanical characteristic representative of the alloy, and complementary optical and scanning electron microscopy for microstructure. The results showed a good corrosion behavior, good superficial resistance, and microstructure properties that could point out some reasons for the interesting results achieved with the evaluated alloy, founding to be potentially used as a biodegradable implant because it exhibited a satisfactory biodegradation rate (0.09 mg cm^{-2}h^{-1})which could prevent their premature rupture during the required period of bone healing.

INTRODUCTION

It is noticeable how the development of medicine and associated technologies strongly influenced the development of new alternatives for surgical implants in recent years. In general terms, implant applicability in a physiological environment mandates that they possess excellent biocompatibility, good mechanical properties, good corrosion resistance, and high resistance to fatigue (Chakraborty Banerjee, 2019). Most of these implants are manufactured by casting metallurgical processes, including casting semi-finished parts, subsequent cold or hot subjection to improve microstructure and mechanical properties, and, finally, net shaping through mechanical activity finishing to meet the dimensional and surface quality requirements (Witte, 2010). But, in recent years, the emerging market for medical devices and surgical implants are opening new possibilities for implants fabricated by powder metallurgy (PM) due to their considerable progress in related manufacturing technologies (Bram, 2013 and Alias, 2019). PM offers the possibility of manufacturing implants with biocompatible elements, well-defined surface roughness or function porosity, combining improved implant fixation due to bone ingrowth, and adaptation of the elastic properties to the human bone, reducing the risk of stress shielding (Bram, 2013). Implants made of biodegradable materials are absorbed and excreted by the body after completing their temporary mechanical, scaffolding,

and bio integration functions (Drelich, 2020). In this group, polymeric, ceramic, and metal materials are included, but metallic biomaterials are notable for higher strength and fracture toughness, meaning they are more suitable for load-bearing applications (Chakraborty Banerjee, 2019). Currently, most of the biodegradable metallic materials are based on magnesium due to its low toxicity and its importance in some biological processes such as muscles, nerves, heart, and influence on the growth of bones, being essential to the human metabolism as a cofactor for many enzymes (Kubásek, 2012). On the other hand, magnesium-based alloys are often characterized by a high corrosion rate in body fluids, which can negatively affect the implant strength during the healing process, leading to a premature implant fracture (Chakraborty Banerjee, 2019; Kubásek, 2012; Virtanen, 2012). For this reason, the search for more alternatives to temporary medical devices and surgical implant material should keep going. In particular, Zinc (Zn), Magnesium (Mg) and Calcium (Ca) alloys are an excellent choice for biodegradable medical devices and surgical implants because all three elements are present in the human body (Fernandes, 2020). Like the Mg, the Zn and Ca have an important role in the human environment as essential elements for humans, relatively high daily allowance (~15 mg for Zn, and ~ 0.8 g for Ca) a large amount of storage (Hou, 2019). As a biodegradable metal, Zn has recently emerged over Mg and Fe. Its corrosion rate is more in line with tissue regeneration. It is also the second most abundant trace metal in the human body, being required for the

development, maintenance, and growth of healthy bones (Cockerill, 2020). As an essential element, Zn is involved in bone metabolism and maintenance of its physiological function and increases osteopathic phosphate activity in bones. Zn is also used as an allowing element to increase the strength and corrosion resistance of Mg alloys. The corrosion rate of pure Zn is lower than that of pure Mg and is not associated with hydrogen gas evolution (Hou, 2019). Additionally, Ca is used as an alloying element in Mg alloys to refine the grains and increase the strength and castability. It is also one of the most important and necessary human bone elements, particularly in terms of chemical signaling with different cells. Moreover, Ca as an inexpensive alloying element with a low density (1.55 g cm^{-3}) similar to the bone can produce hydroxyapatite (HA) during the corrosion in the body and accelerate bone healing (Harandi, 2012). Different alloys using Zn, Mg, and Ca as components have already been addressed in previous studies in the majority, keeping the amount of Zn and Ca as alloying elements in a low percentage in Mg-based alloys. Still, none of them using PM on their method (Cha, 2013; Ding, 2019; Jiang, 2019; Annur, 2016). The comprehensive studies of these works highlight the interactions between corrosion and mechanical integrity and the fatigue behavior of materials and suggest the importance of investigating overall properties when new alloys are developed and evaluated for practical applications. In this study, powder metallurgy (PM) was used to fabricate an alloy using Zn, Mg, and Ca on its composition, Zn-42Mg-4Ca. Mechanical properties of the alloy followed by microstructure analyses, electrochemical and degradation evolution were carried out to compare the obtained results with other known alloys from the literature, checking its viability to be used in degradable surgical implants.

After removed from the furnace, the samples had their densities checked considering their final weight and dimensions. All these steps are summarized in Fig.1.

Microstructure characterization: The microstructural observations of samples in all states were performed on cross-sections perpendicular to pressing direction, prepared by grinding with silicon carbide papers up to #2500 grid and polishing with 1μm alcohol-based diamond suspensions. Light optical microscopy (LOM) and scanning electron microscopy (SEM) were used to evaluate morphologies and phases. An optical microscope (Olympus BX51M; Olympus, Tokyo, Japan), coupled with the Olympus SC30 digital camera, was used with the stream basic software (Olympus, 8.1, Tokyo, Japan) to acquire images. For SEM analyses, an FEI equipment model Inspect S50, coupled with a tungsten filament and EDX-EDAX and a Zeiss-EVO-10 with secondary electrons detector Jeol JSM-5800, was used. The microstructural observation and morphology characterization were performed at an open voltage of 20kV. The volume fraction of the second phases and porous percentage were measured using the ImageJ software.

Mechanical properties: The alloy's mechanical properties were evaluated using a dynamic ultra-microhardness tester (DUH) (Shimadzu DUH-211S) at room temperature. Individual tests were assessed on the transverse section, and the averaged values were recorded for the discussion. The DUH measurements were performed using a 115º triangular pyramid indenter with a test force rate (load/unload) of 7 gf s^{-1} until the maximum load of 30 gf and dwell time of 10 s before releasing the load.
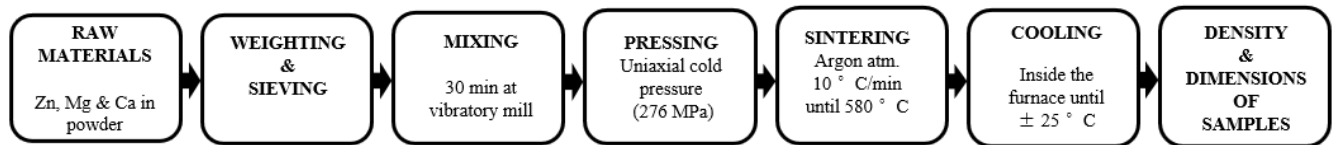

Fig. 1. Production procedure of the samples adopted in this study

Table 1. Chemical composition of Kokubo solution used as SBF in this study (g L^{-1})

Solution	NaCl	Na$_2$HCO$_3$	KCl	KH$_2$PO$_4$ * 3H$_2$O	MgCl$_2$ 6H$_2$O	HCl	CaCl$_2$	Na$_2$SO$_4$	CH$_2$OH$_3$CNH$_2$
Kokubo	7.996	0.350	0.224	0.228	0.305	40 ml	0.278	0.071	6.057

MATERIALS AND METHODS

Materials processing and alloy fabrication: To fabricate the Zn-42Mg-4Zn alloy samples, elemental powders of pure Zn, Mg, and Ca were furnished by the Military Chemical Laboratory (LQM) of the Brazilian Army of Technological Center (CTEx). The powders' purity levels were measured using the spectrometer of fluorescence of x-rays (BRUKER - Model S8 Tiger/Software Spectra Plus 2.4.0.8). The powders were then sieved in a vibrating machine model "T" and sieves from the Tyler series (Produtest brand). The sieving time adopted was 30 min for each powder using the potentiometer of the vibrating machine in the "eight" position. Posteriorly, the material retained in each sieve was weighed. As a standard, the powder's dimension was correspondent to the sieve, where the powder quantity in weight was mainly retained. This procedure was repeated at least three times for each powder using 50 g each time. To prepare the alloy samples, the powders was weighed using a precision digital balance with a resolution of 0.001 g (Marte, AY220). The powders were mixed for 30 min in a vibratory mill (Retsch model, MM-400) at a frequency of 15 Hz. Then, the compactions of the mixed powders were obtained by pressing them under a uniaxial load of 276 MPa using a die with a rounded surface with 74.5 mm^2 at room temperature and a total compact volume of approximately 1.3 cm^3. After trials, these parameters were selected to obtain adequate green compact for sintering under a controlled environment inside the Netzsch-Dill 402C dilatometer cabin. After the compaction procedure, the green samples were sintered in an argon environment at a temperature rate of 10 °C per min until 580 °C and then maintained at a constant temperature for 60 min and cooled down inside the furnace to room temperature ±25 °C.

After standard sample surface preparation, in which the samples were ground using silicon carbide papers until 2500#, the test evaluation was performed by entering the indenter on the sample surface. By this evaluation, the alloy resistance information as yield strength, elastic modulus, the deep penetration, and the Vickers hardness, can be reached with a high degree of confidence in accordance with ISO standard 14577-1- Annex A.

Corrosion experiments: The produced samples' corrosion behavior was evaluated by checking the potential-dynamic polarization curve (PPC) and the degradation rate (DR) curves of the alloys. The samples were tested in a simulated body fluid (SBF) termed Kokubo solution [17]. This solution was prepared under laboratory conditions according tothe presented in Table 1. To account for the human physiological conditions, the pH of SBF was adjusted to 7.4, and the temperature was maintained at 37 °C ± 1.0 °C. These parameters were frequently monitored and kept constant during all the corrosion tests buffering with tris-hydroxymethyl aminomethane ((CH$_2$OH$_3$)CNH$_2$) to pH control.

Electrochemical evaluations: The electrochemical evaluations of specimens by PPC were carried out using an electrochemical workstation (Autolab PGSTAT204 – Metrohm) and data collected by NOVA 2.1 interface software. For the three-electrode cell, a saturated calomel cell was used as a reference electrode (SCE), a platinum cell as a counter electrode (CE) with a surface area of 1.0 cm^2, and the fabricated alloy sample in the center as the working electrode (WE). All those components were put inside a graduated beakerwith 100 mL of SBF. The SBF temperature was controlled at 37°Cby a digital thermostat W1209 with a hysteresis of ± 2 ° C. with a 500 W

resistance heater. The open-circuit potential (E_{ocp}) of each sample was tested at first. Then the potentiodynamic polarization test was carried out at a constant scanning rate of 300 mV s^{-1}. The tests were performed three times for each specimen to obtain the representative results. The current densities (i_{corr}) and the corrosion potentials (E_{corr}) were obtained through graphical Tafel analysis, and the relationship between i_{corr} (mA cm^{-2}) and the electrochemical degradation rate (mm year^{-1}) is described as the Eq. 6 (Delgado, 2017 and Shi, 2011).

$$P_i = 22.85\, i_{corr} \qquad (1)$$

Degradation rate evaluation: For the degradation rate evaluation, the hydrogen (H$_2$) evolution was monitored and converted to the sample degradation rate (DR) using mass balance. The apparatus prepared to measure the hydrogen evolution during the time of exposition within the corrosion environment was set up in accordance with the ASTM-G31-72 standard. This configuration allowed for collecting the hydrogen bubbles generated from the soaked sample enabling the measurement of alloy hydrogen evolution by calculating the height difference of the simulated body fluid used inside the measuring cylinder using a precision weight balance. The tests were performed with a total volume of 400 mL and a resolution of 1.0 mL. The fabricated samples were ground using silicon carbide papers until 2500#, immersed in SBF at 37.0 ± 2 °C, and pH around 7.4. Approximately 50mL SBF per square centimeter of the sample surface was used during the ten days (240h) of the experiment, and three samples were used for the sake of reproductivity. As the sample degradation starts, an increase in pH is noticed, which may affect the degradation rate, thereby requiring the solution to be refreshed every 24 h. The same protocol was used for all measurements to compensate for this effect. After different immersion times, the soaked specimens were rinsed with ethyl alcohol and dried under cool air. Then, the alloy degradation rate was estimated based on the immersion time and hydrogen evolution by converting the total collected hydrogen into a material loss, being expressed in millimeters per year by using Eq. 7.

$$DR = \frac{8.76 * 10^4 * \Delta g}{A * t * \rho} \quad (\text{mm year}^{-1}) \qquad (2)$$

where Δg is the weight change (g), A is the sample surface area (cm^2), t is the immersion time (h), and ρ is the density of the fabricated alloy (g cm^{-3}).

RESULTS

Powder characterization: The results of the purity levels of Zn, Mg, and Ca powders obtained by X-ray fluorescence is presented in Table 2:

Table 2. Level of purity of each initial powder used in this study

Mg Powder		Zn Powder		Ca Powder	
Elements	m/m. %. Max.	Elements	m/m. %. Max.	Elements	m/m. %. Max.
Mg	98.22	Zn	99.74	Ca	99.57
P	0.606	Ca	0.187	Mg	0.137
Ca	0.329	P	0.120	Cl	0.057
Si	0.449	Ta	0.111	W	0.063
Mn	0.088	Si	0.080	Sr	0.060
Zn	0.047	Al	0.040	P	0.050
S	0.124	Fe	0.021	Si	0.038
K	0.059	Cu	0.021	Fe	0.016
Fe	0.040	Ag	0.013		
Cu	0.020				
Ni	0.016				

The dimensions of the powders were obtained through the sieving process. The Zn powder was more retained on Tyler sieve 500, which corresponds to 0.025 mm of powder dimension. The Mg powder was more retained on Tyler sieve 120, corresponding to 0.125 mm, and for Ca powder, the Tyler sieve more retained was the 35, which corresponds to 0.500 mm of dimension. To ensure good uniformity,

only sieved powders were used in the fabrication of the Zn-42Mg-4Ca alloy.

Fabricated alloys: In powder metallurgy, the sintering process promotes increasing particle contact due to the formation of bonding between atoms. The dilatometer can help to track this phenomenon. In this study, five samples of the evaluated alloy with approximately the same dimensions in diameter and height (Ø 9.8mm x 17.5mm) were fabricated by sintering processin the Netzsch-Dill 402C dilatometer. The fabricated samples and the dilatometer curve are depicted in Figs.2 a and b, respectively.The densities of the fabricated alloys were checked considering their final weight and dimensions. The densities were 1.832 g/cm^3 ± 0.240 on average. These values are potentially good, considering the effects of stress shielding between bone and implant. They are similar to the natural human bone density (1.8 g/cm^3 to 2.1 g/cm^3 depending on the bone structure) (Peron, 2020).
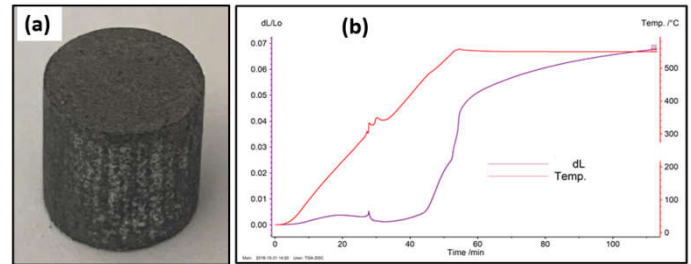

Figure 2. Image of sintered Zn-42Mg-4Ca sample (a) and the correspondent dilatation curve during the sintering process (b)

Microstructure Characterization: The microstructures of the evaluated alloy are presented in Fig. 3. Fig. 3a is representative of the LOM, no-etching. The feature exhibited is close to a dendritic microstructure and intermetallic compounds at interdendritic regions. The powder metallurgy parameters during the sintering process have certainly influenced the alloy feature, producing some level of porosity due to the different sizes and melting point of alloying elements. Fig. 3b shows the alloy surface's microstructure already presenting some corrosion attack, mostly in the form of corrosion cavities of various sizes (black arrows) and some pores (red arrows). Probably its corrosion attack manifested itself during the sample preparation process, where contact with water is inevitable. Some isolated α-Mg phases are also observed. Fig. 3c depicts the EDS map of element distribution in the alloy. For a certain region of the sample, where the presence of oxygen confirms the eminent corrosion film installed on the surface. Evidently, the presence of Mg and Ca in the alloy formed a solid solution in the Zn matrix, allowing for the formation of precipitate in the second phase and lamellar eutectic in the microstructure. The lamellar eutectic structures were mostly distributed inside the grain boundary and less distributed in the inter-dendrite areas. Considering the alloy composition (Zn-42Mg-4Ca), it was expected that the secondary phases were mostly Mg$_4$Zn$_7$, Mg$_7$Zn$_3$, and Mg$_2$Zn$_{11}$. However, the alloy's Ca content can also contribute to the formation of Mg-Zn-Ca phases with distinct compositions as Ca$_2$Mg$_6$Zn$_3$ (Annur, 2016 and Du, 2018). Additionally, two areas identified as "A" (inside a grain) and "B" (in the grain border) are detached in Fig. 3b (white square areas), also shown in Fig. 3d and Fig. 3e with higher amplification. Inside these areas, the chemical composition of points 1 and 2 was determined by EDS analysis, and the spectra are shown simultaneously. The EDS result of point 1 in the alloy was Mg-36.19 at.%Zn resulting in the atomic ratio of Mg/Zn in ~1.86, which is close to the composition of the Mg$_7$Zn$_3$or Mg$_2$Zn$_{11}$ phase. For point 2, Ca's presencemay lead the secondary phases to transform from the Mg$_7$Zn$_3$ phase and the Mg$_2$Zn$_{11}$phase into the Mg-Zn-Ca phase distributed along grain boundaries. It was reported that the type of the second phase was related to the Zn/Ca atomic ratio in Mg-Zn-Ca based alloys where the atomic ratio of Zn/Ca more than 1.25 generally lead to the phase consisting of α-Mg solid solution and Mg-Zn-Ca phase (Ca$_2$Mg$_6$Zn$_3$) (Annur, 2016). The influence of Ca content on the microstructure of the alloy prepared in this study affected the lamellar eutectic appearance of the alloy's microstructure. Zhang *et al.* (2011) have confirmed this trend in a previous study by changing the
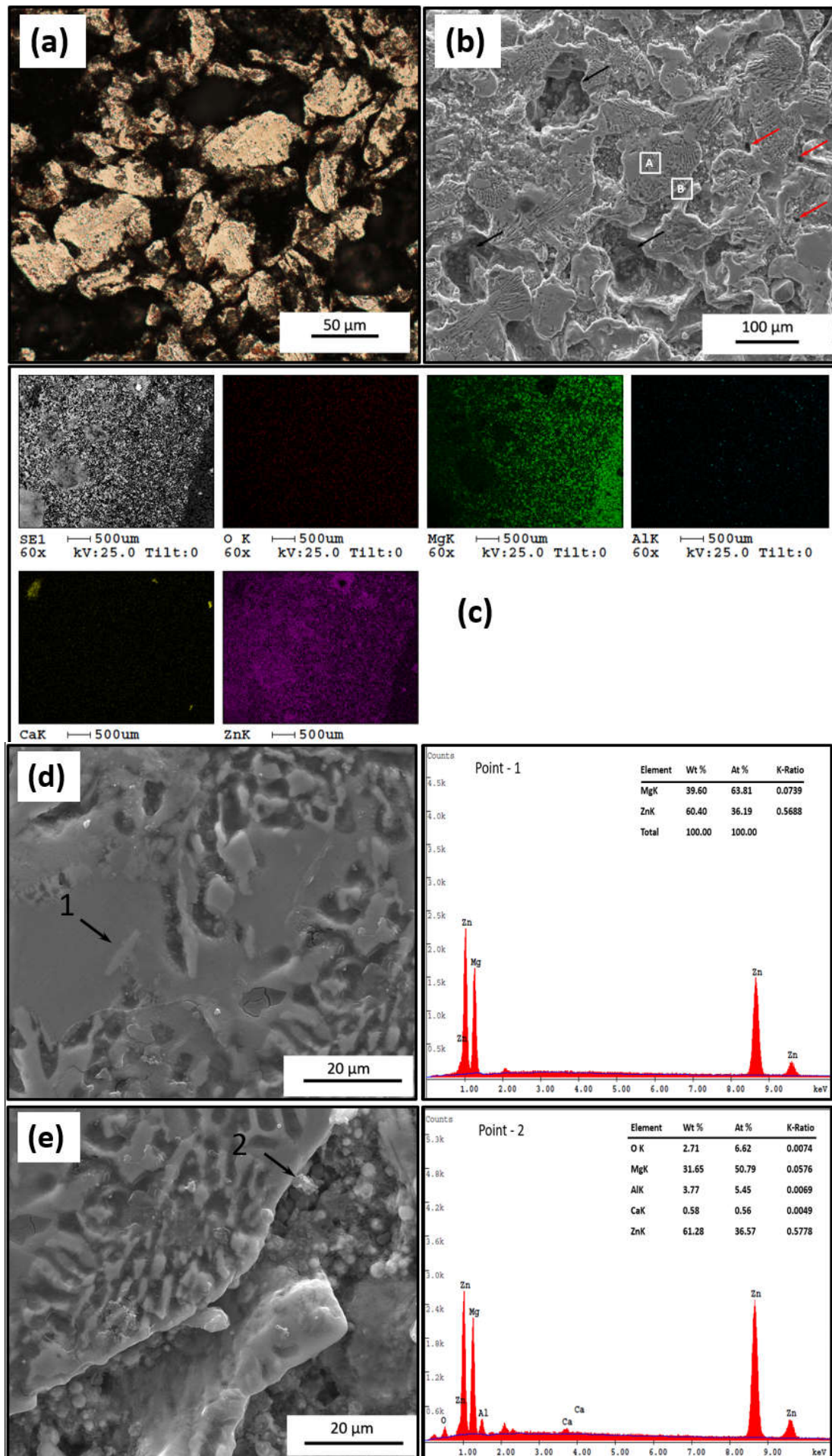
Fig. 3. The optical micrograph of Zn-42-4Ca alloy, no-etching (a), SEM micrograph (b), SEM micrograph with the element map distribution obtained from the alloy (c), SEM micrograph of the area "A" and the EDS chemical analysis of the Point 1 (d), SEM micrograph of the area "B" and the EDS chemical analysis of the Point 2 (e)

Ca content in Mg-Zn-Ca alloys and further evaluating their microstructure morphologies via SEM analyses. Clearly, as the Ca content increases in the alloy composition, the second phase's morphogenesis changes from the polygonal form to small round particles and further to a lamellar structure when the Ca content is significantly higher. The lamellar structure confirms the combined effect of the Ca in the alloy, which could favor the formation of different phases and morphology, which can influence both mechanical and biocompatibility properties. However, further study of these suspicions is beyond this study's context and might be conducted in new research.

Mechanical properties evaluation: Typical curves of an individual indentation load versus penetration depth by DUH tester for Zn-42Mg-4Ca alloy are presented in Fig. 4. Table 2 is summarizing the individual tests, and the average values are shown in the same table. Some additional information as the plastic deformation (h_p) with total deformation (h_t) ratio and elastic deformation (h_e) with total deformation (h_t) ratio is additionally presented.
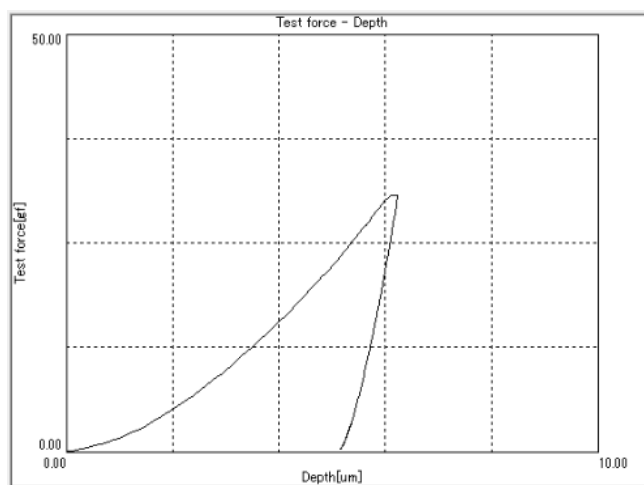
presented in Fig. 5. Each measured for a separate specimen after solution immersion for the stated time. The samples exhibited a very fast corrosion potential, and their maximum and stable potential were achieved after a short time of exposition in the SBF. The cathodic polarization curves represent the evolution of cathodic hydrogen as a result of water reduction. At the same time, the anodic polarization curves represent the dissolution of the alloy and the passivation tendency, indicating the formation of oxide films on the alloy surface (Du, 2018; Cai, 2012 and Song, 2012). The alloy's corrosion potential was -1484 mV, indicating that the alloy's electrochemical reactions took place in electrode/solution interfaces, suggesting that the alloy exhibited a low susceptibility to an electrochemical reaction. The corrosion potential value (i_{corr}), which is also inferred from the curve, is directly proportional to the corrosion rate showing avalue of 0.09mA cm^{-2}on average. It is expected that the combination of the highest E_{corr} and lower i_{corr} yields the best corrosion performance of the materials.The dissolution rates increased, attain a maximum value, and decrease to a very low value. The potential increase had little effect on the current in the passive region until the passivity breaks down.
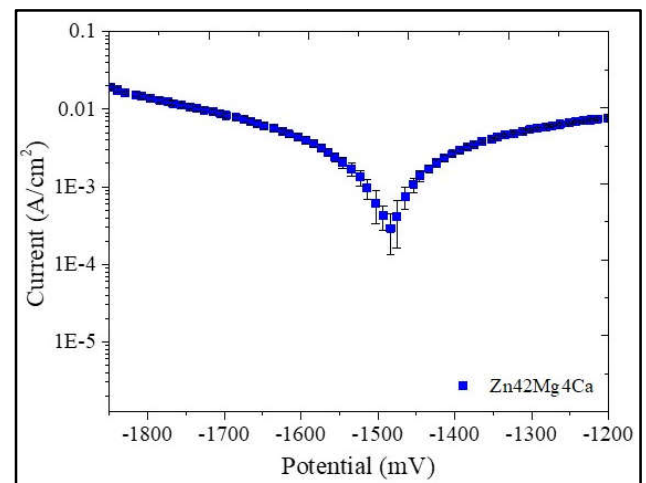

Fig. 4. Load-indentation depth curve for Zn-42Mg-4Ca alloy obtained from DUH test

Fig. 5. Polarization curves for Zn-42Mg-4Ca alloy

Table 3. DUH values obtained for the Zn-42Mg-4Ca alloy.

Test	F_{max} (gf)	Total deformation h_t (μm)	Plastic deformation h_p (μm)	Elastic deformation h_e (μm)	h_p / h_t (%)	h_e / h_t (%)	H_{it} (MPa)	HV* (HV)	E (GPa)
1	30.55	7.186	6.309	0.877	88	12	276.9	26.2	10.7
2	30.79	5.417	4.461	0.956	82	16	521.0	49.2	14.3
3	30.53	6.591	5.573	1.018	85	15	341.2	32.2	10.5
4	30.75	4.902	3.906	0.996	80	20	665.5	62.9	14.8
5	30.68	6.254	5.165	1.089	83	17	387.3	36.6	10.9
Average	30.66	6.067	5.083	0.984	84	16	438.4	41.4	12.2

The average elastic modulus (12.2 GPa) and the superficial hardness (41.4 HV) obtained for the evaluated alloy are in compliance with those of natural bone, which can avoid the stress shielding occurrence during the bone healing process (Chakraborty, 2019 and Gao, 2018). Stress shielding occurs when a healing bone experiences stress below a necessary threshold because of the implant material. Consequently, the closer the alloy's mechanical properties are to those of natural bones, the better chance of success on the bone healing treatment. The average yield strength (438.4 MPa) obtained for the fabricated alloy shows a good resistance. Additionally, its ductility could be confirmed because the plastic deformation ratio versus the total deformation (84%)was much higher than the ratio of the elastic deformation versus the total deformation (16%), which is in good agreement with ductile material. All these results have confirmed the good mechanical properties of the fabricated alloy to implant material.

Corrosion evaluations

Electrochemical corrosion evaluations: The average values of the potentialdynamic polarization curve for the Zn-42Mg-4Ca alloy are

The current rises rapidly, with the potential indicating a localized corrosion trend. Additionally, the relationship between the i_{corr}(mA cm^{-2}) and the electrochemical corrosion rate (mm year^{-1}) was calculated, obtaining a value of 2.06± 0.6 mm year^{-1}.

Degradation rate of the alloy: The average result for the immersion test (hydrogen evolution) is depicted in Fig. 6. The results are expressed in terms of hydrogen evolution per hour until 240 h in SBF solution. The values were expressed in mL cm^{-2}, and three samples were tested under the same conditions to sake the results (Zhang, 2011 and Song, 2011). The values of hydrogen evolution during the first 48 h in SBF was extremely high, as Fig. 6 shows. Also inferred from the curve, it couldbe seen thatthe hydrogen evolution hada trend to stabilize, after the 72 h,achieving the largest volume of H$_2$, i.e., 21.35 ml cm^{-2} corresponding to 4.61±0.23 mm year^{-1} which,did nottotally agree to the electrochemical test results reported. The alloy's degradation exhibited favorable behavior in that they maintained their mechanical structure during the 240 h of exposure to the SBF solution. These results have suggested that the alloy will exhibit corrosion properties in compliance with the required structural

function during the period of the fractured bone trauma consolidation, which is usually 12 weeks (Witte, 2004).
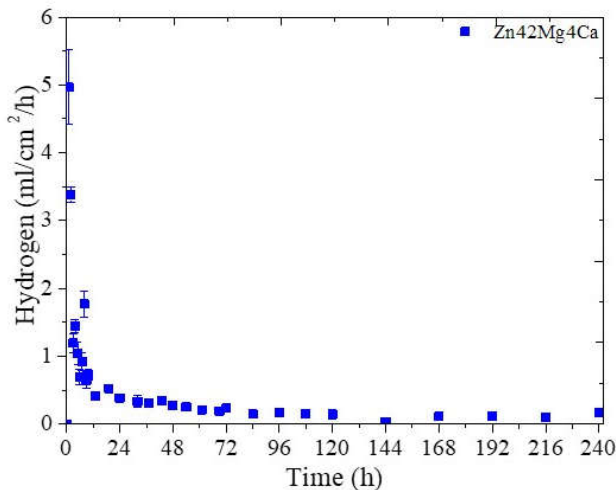

Fig. 6. Hydrogen evolution in Zn-42Mg-4Ca alloy

DISCUSSIONS

Powder metallurgy effects: Bram et al. [3] reported that PM is an attractive alternative under economic considerations if many complex-shaped parts are required. Additionally, PM might become advantageous for lightweight metallic biomaterials, which are difficult to machine by conventional methods. The possibility of manufacturing bone implants with well-defined surface roughness or function porosity is also an advance because it can reduce the risk of stress shielding, combining improved implant fixation due to the bone ingrowth and adaptation of the elastic properties to the human bone. For the Zn-42Mg-4Ca alloy evaluated,Fig.3 (a) shows pores and neck regions with a good degree of cohesion. Increased porosity (pores volume fraction) was expected as the Ca content increases in the alloy [16]. Optical quantitative metallographic analyses revealed that the pores volume fraction of the fabricated Zn-42Mg-4Ca alloy was 56%, confirming this feature. Oliveira et al.[28]commented that higher interconnected porosity is crucial for biocompatibility and is usually associated with higher connectivity between bone and implant. Porosity degrees of at least 60% would lead to an interconnected porous structure, which favors the cell ingrowth to porous space, vascularization, and transport of metabolic products. Schaper et al. [30], during the AZ81 Mg alloy evaluation for powder metal injection moulding (MIM), reported that the aspect and the average grain size of the formed alloy arealso related to the sintering process (Fig. 3 (b)) due to the different chemical elements used and their sizes.These parameters can be controlled and changed, depending on the balance of the properties required for the alloy, and will be an object of further verification.

Mechanical properties effect: To comparison on further discussion, the obtained properties of Zn-42Mg-4Ca alloy and other biodegradable alloys were summarized in Table 4. It is worth to say that, even having pores, the fabricated alloy presented an adequate level of resistance, adherent to that of the natural bone. Additionally, the mechanical properties of the alloy are revealed like other known biodegradable metallic implants. The strength of the studied alloy can be associated with Zn's ductility and, to a certain extent, the ductility of Mg also presents in the alloy composition. Both elements have a hexagonal close-packed (hcp) crystalline structure that lacks a slip system active at room temperature, impacting alloy deformability (Bian, 2016). This inherent alloy feature is depicted in table 3, where the h_p/h_t ratio is about 84% on average. Considering the yield strength of the Zn-42Mg-4Ca alloy compared to the others, a big range of values could be noticed indicating a variation that can be related to the presence of pores in the alloy also the cohesion between the chemical elements during the sintering process. The obtained results for superficial hardness (Vickers analyses) followed the same characteristic, confirming the trend (Hao, 2009). Further, the

mechanical resistance of the evaluated alloy can also berelated to the precipitation of secondary phases presents (Fig.3 (d) & (e)). The second phase may considerably improve the alloy strength because it hinders the dislocation reduction, and its dispersion at the grain boundary increases the dislocation density of the alloy (Cai, 2012).

Corrosion effects: As known, the human body fluid consists of water, electrolytic ions as chlorine, sodium, and more, proteins, and dissolved oxygen. This environment is extremely aggressive to metals in general, where the corrosion process takes place in an electrolytic way, most of the time, forming hydroxides (Witte, 2010). It is expected that the formed hydroxide layer covers the surface of the alloys making a kind of barrier that will reduce the corrosion process. But it is also known that this hydroxide layer is not stable in the presence of chloride ions in the human body fluid commented that a multiple layer mainly consisted of O, C, P, Mg, and Ca elements is formed upon immersion into an SBF solution, where the alloys react (cathodic reaction) because of galvanic corrosion between matrix and the secondary phase companying with the hydrogen evolution. This reaction leads to a thin heterogeneous porous layer mainly composed of $Mg(OH)_2$. Therefore, the increased amount of second phase particles is believed to enhance the galvanic corrosion between the Mg matrix and the second phase, thereby promoting the alloy's degradation (Hou, 2019). This phenomenon hastens the corrosion of the alloys. The hydrogen evolution during its corrosion can create subcutaneous gas bubbles in the fractured region that can cause the separation of tissues and/or tissues layers that can deterioratethe bone healing (Chakrabordy, 2019). In the present study, the fabricated alloy has a low content of second phase particles, and its matrix is richer in Zn than Mg, as shown in matrix mapping in Fig. 4(c). This characteristic may reduce the galvanic corrosion and is adherent with Fig. 6. In this context, compared to other biodegradable implant materials, zinc alloys can assume a better position. The zinc electrochemical potential is -0.76V, and because of that, it can significantly reduce the corrosion process of their alloys without losing the potential to be totally degradable with time. Hou et al., investigating Mg-Zn-Ca alloys with low content of Zn (0.7 wt%) and Ca (0.6 wt%) in different process conditions, observed that Mg_2Ca particles in the alloy are dissolved as local anodes due to its higher activity than Mg in the matrix, which combined with the release of Zn, lead to the accumulation of Ca2+ and Zn2+ in the medium resulting in the increase of resistance of the alloy during the immersion time exposure in SBF. Bakhsheshi-Rad et al. investigated Mg-0.5Ca-xZn alloys and found that the alloys' corrosion resistance increased due to the formation of Mg-Zn-Ca phases and Mg_2Ca phases. Abdel-Gawad and Schoeib found that the Mg-Zn-Ca phase inhibited the local corrosion by acting as a temporary local corrosion barrier against the corrosion attack of the matrix. Still, it was also a cathodic site for the matrix phase as immersion time extended.

Therefore, the corrosion resistance of the Zn-42Mg-4Ca alloy may also be related to the Mg-Zn-Ca phase presence, as depicted in Fig. 4 (e). As comparison, some previous investigations in biodegradable implant corrosion were summarized in Table 5. The potential-dynamic polarization curve conducted for the Zn-42Mg-4Ca alloy (Fig.5) suggested a formation of a protect film on the alloy surface after a short time in SBF with undoubtedly passivation stage. The corrosion potential (mV) at the investigated alloy was the lowest compared to the others but higher than pure Mg. The alloy (mA cm^{-2}) corrosion current density was more sensitive and identical to the pure Mg, indicating a high result on the alloy degradation. The hypothesis put forth for this is the greater capacity for forming a passivation coating on this alloy due to the Zn oxidation on the sample surface at the beginning of the exposition in SBF, which is adherent with the degradation curve for the alloy, depicted from Fig. 6. Moreover, a passivation film seems to be formed and maintain continuous and controlled dissolution during the time, which is a favorable property for its bio-absorption and application to self-absorption implants. It is worth to say that the hydrogen evolution of the studied alloy was extremely high in the beginning times, achieving a value around 5 ml cm^{-2} h^{-1} but, over time, this phenomenon is reduced to a constant value close to 0.09ml cm^{-2} h^{-1}. As a target, in-vitro studies have reported the critical tolerance level of hydrogen gas should be lower

Table 4. A comparison of the mechanical properties of biodegradable metallic implants and natural bone

Property	Natural bone	Mg-4Zn-0.2Mn	AZ31	ZM20	Zn-42Mg-4Ca [author]
Density (g cm^{-3})	1.8 – 2.1	1.74 – 2.0 [1]	1.74 – 2.0 [1]	1.74 – 2.0 [1]	1.59 – 2.07
Elastic Modulus (GPa)	3 - 20	-	-	32.1 – 32.7	10.5 – 14.8
Yield Strength (MPa)	130 - 180	56	92.6 – 102.5	538.7– 558.5	276.9 – 669.5
Hardness (HV)	26.2 – 42.1	-	60.0 – 70.2	49.8 – 51.6	26.2 - 62.9

Table 5. A comparison of the corrosion evaluations of some biodegradable metallic implants and the alloy Zn-42Mg-4Ca

Conditions	Pure Mg	Mg-4Zn-0.2Mn	AZ31	ZM20	Zn-42Mg-4Ca [author]
Immersion time (h)	720	960	100	240	240
SBF (solution)	Hank	Hank	Kokubo	Kokubo	Kokubo
P_i (mm/year) [1]	2.08 ± 0.2	0.68 ± 0.07	0.06 [3]	0.16 [3]	2.06 ± 0.9
Corrosion rate (mm/year) [2]				1.80 ± 0.12	4.61 ± 0.23
Potential (mV)	-1276	-1559	-1830	-1764	-1484
Current (mA/cm^2)	0.09 [3]	3.07 x 10^{-3}	2.55 x 10^{-3}	6.88 x 10^{-3}	0.09 ± 0.02

(1) Calculated by dynamic polarization curve
(2) Calculated by H$_2$ dissolution
(3) Calculated by the author

than 0.01mlcm-^{2}day^{-1}, and this has been widely used to screen all the temporary implant materials (Song, 2011). The Zn-42Mg-4Ca alloy degradation rate stabilized at close to 2.1 mg/cm^2/day which is consistent with findings from previous other studies on biodegradation alloys with additional mechanical, thermal, and coating treatments (Delgado, 2017; Peron, 2020; Song, 2011; Witte, 2004; Li, 2013 and Witte, 2009), for example, inferred that the weight loss result of pure Mg alloys evaluated under similar conditions was close to 3.6 mg/cm^2/day, which is much higher. The alloy's degradation rate was significantly lower after 72 h of exposure in SBF solution (Fig. 6) keeping continued to degrade at a rate of 0.06 mm/year after this period, which is like the AZ31 alloy showedin Table 5. Based on the evidence of these corrosion analyses, the studied alloy maintained its structural state for a significant time, exhibiting a good corrosion resistance, and to the chemical effect reduction, further preserving its metal base and presenting lower sensitivity to ions such as Cl-, HPO42-, HCO3-, and SO42- in the physiological solution.

Conclusion

A biocompatible alloy was successfully fabricated by powder metallurgy with the composition of Zn-42Mg-4Ca. Its microstructure, mechanical properties, superficial electrochemical behavior, and degradability in SBF were evaluated compared with some other recognized biodegradable alloys. Based on the obtained results and discussions, the alloy presented a good mechanical resistance, in line with the bone resistance, preventing the stress shielding issues. Additionally, its microstructure showed the presence of second phases, which may considerably improve the strength while decreasing the alloy's plasticity. Finally, the alloy's corrosion evaluation has confirmed an adequate degradation rate that indicates the great potential of Zn-42Mg-4Ca alloy for biodegradable implant material.

REFERENCES

B. P. Zhang, Y. Wang, e L. Geng, "Research on Mg-Zn-Ca Alloy as Degradable Biomaterial", in *Biomaterials - Physics and Chemistry*, R. Pignatello, Org. InTech, 2011.

B. Yin, J. Guo, J. Wang, S. Li, Y. Liu, e Y. Zhang, "Bone Material Properties of Human Phalanges Using Vickers Indentation", *Orthop. Surg.*, vol. 11, n° 3, p. 487–492, jun. 2019, doi: 10.1111/os.12455.

C. S. S. de Oliveira, S. Griza, M. V. de Oliveira, A. A. Ribeiro, e M. B. Leite, "Study of the porous Ti35Nb alloy processing parameters for implant applications", *Powder Technol.*, vol. 281, p. 91–98, set. 2015, doi: 10.1016/j.powtec.2015.03.014.

D. Annur, F. P. L., A. Erryani, M. I. Amal, L. S. Sitorus, e I. Kartika, "The synthesis and characterization of Mg-Zn-Ca alloy by powder metallurgy process", Semarang, Indonesia, 2016, p. 020032, doi: 10.1063/1.4945486.

D. Bian, W. Zhou, Y. Liu, N. Li, Y. Zheng, e Z. Sun, "Fatigue behaviors of HP-Mg, Mg–Ca and Mg–Zn–Ca biodegradable metals in air and simulated body fluid", *Acta Biomater.*, vol. 41, p. 351–360, set. 2016, doi: 10.1016/j.actbio.2016.05.031.

F. Witte *et al.*, "Degradable biomaterials based on magnesium corrosion", *Curr. Opin. Solid State Mater. Sci.*, vol. 12, n° 5–6, p. 63–72, out. 2008, doi: 10.1016/j.cossms.2009.04.001.

F. Witte *et al.*, "In vivo corrosion of four magnesium alloys and the associated bone response", *Biomaterials*, vol. 26, n° 17, p. 3557–3563, jun. 2005, doi: 10.1016/j.biomaterials.2004.09.049.

F. Witte, "The history of biodegradable magnesium implants: A review☆", *Acta Biomater.*, vol. 6, n° 5, p. 1680–1692, may 2010, doi: 10.1016/j.actbio.2010.02.028.

G. L. Hao, F. S. Han, e W. D. Li, "Processing and mechanical properties of magnesium foams", *J. Porous Mater.*, vol. 16, n° 3, p. 251–256, jun. 2009, doi: 10.1007/s10934-008-9194-y.

G.-L. Song, Org., *Corrosion of magnesium alloys*. Oxford; Philadelphia, PA: Woodhead Publishing, 2011.

H. R. Bakhsheshi-Rad, M. R. Abdul-Kadir, M. H. Idris, e S. Farahany, "Relationship between the corrosion behavior and the thermal characteristics and microstructure of Mg–0.5Ca–xZn alloys", *Corros. Sci.*, vol. 64, p. 184–197, nov. 2012, doi: 10.1016/j.corsci.2012.07.015.

I. Cockerill *et al.*, "Salt Preform Texturing of Absorbable Zn Substrates for Bone-Implant Applications", *JOM*, vol. 72, n° 5, p. 1902–1909, may 2020, doi: 10.1007/s11837-019-03971-1.

J. Alias, W. S. W. Harun, e H. M. Ayu, "A Review on the Preparation of Magnesium-Based Alloys Prepared by Powder Metallurgy and the Evolution of Microstructure and Mechanical Properties", *Key Eng. Mater.*, vol. 796, p. 3–10, mar. 2019, doi: 10.4028/www.scientific.net/KEM.796.3.

J. G. Schaper, M. Wolff, B. Wiese, T. Ebel, e R. Willumeit-Römer, "Powder metal injection moulding and heat treatment of AZ81 Mg alloy", *J. Mater. Process. Technol.*, vol. 267, p. 241–246, may 2019, doi: 10.1016/j.jmatprotec.2018.12.015.

J. Kubásek e D. Vojtěch, "Zn-based alloys as an alternative biodegradable materials", *Met. 2012 - Conf. Proc. 21st Int. Conf. Metall. Mater.*, vol. 5, p. 1355–1361, jan. 2012.

J. M.Rúa, A. A. Zuleta, J. Ramírez, e P. Fernández-Morales, "Micro-arc oxidation coating on porous magnesium foam and its

potential biomedical applications", *Surf. Coat. Technol.*, vol. 360, p. 213–221, fev. 2019, doi: 10.1016/j.surfcoat.2018.12.106.

J. W. Drelich *et al.*, "Biodegradable Materials for Medical Applications II", *JOM*, vol. 72, n° 5, p. 1830–1832, may 2020, doi: 10.1007/s11837-020-04129-0.

K. Prasad *et al.*, "Metallic Biomaterials: Current Challenges and Opportunities", *Materials*, vol. 10, n° 8, p. 884, jul. 2017, doi: 10.3390/ma10080884.

M. Bram, T. Ebel, M. Wolff, A. P. Cysne Barbosa, e N. Tuncer, "Applications of powder metallurgy in biomaterials", in *Advances in Powder Metallurgy*, Elsevier, 2013, p. 520–554.

M. C. Delgado, F. R. García-Galvan, I. Llorente, P. Pérez, P. Adeva, e S. Feliu, "Influence of aluminium enrichment in the near-surface region of commercial twin-roll cast AZ31 alloys on their corrosion behaviour", *Corros. Sci.*, vol. 123, p. 182–196, jul. 2017, doi: 10.1016/j.corsci.2017.04.027.

M. Peron *et al.*, "The effect of Equal Channel Angular Pressing on the stress corrosion cracking susceptibility of AZ31 alloy in simulated body fluid", *J. Mech. Behav. Biomed. Mater.*, vol. 106, p. 103724, jun. 2020, doi: 10.1016/j.jmbbm.2020.103724.

M. T. Fernandes, L. M. da Silva, B. X. de Freitas, G. Domingues, J. A. de Castro, e C. dos Santos, "Effects of Zn content on surface deformability and corrosion resistance of MgZnMnCa alloys", *Int. J. Mater. Res.*, vol. 111, n° 6, p. 511–518, jun. 2020, doi: 10.3139/146.111908.

N. Li e Y. Zheng, "Novel Magnesium Alloys Developed for Biomedical Application: A Review", *J. Mater. Sci. Technol.*, vol. 29, n° 6, p. 489–502, jun. 2013, doi: 10.1016/j.jmst.2013.02.005.

P. Chakraborty Banerjee, S. Al-Saadi, L. Choudhary, S. E. Harandi, e R. Singh, "Magnesium Implants: Prospects and Challenges"*Materials*, vol. 12, n° 1, p. 136, jan. 2019, doi: 10.3390/ma12010136.

P. Ding, Y. Liu, X. He, D. Liu, e M. Chen, "In vitro and in vivo biocompatibility of Mg–Zn–Ca alloy operative clip", *Bioact. Mater.*, vol. 4, p. 236–244, dez. 2019, doi: 10.1016/j.bioactmat.2019.07.002.

P. Jiang, C. Blawert, R. Hou, J. Bohlen, N. Konchakova, e M. L. Zheludkevich, "A comprehensive comparison of the corrosion performance, fatigue behavior and mechanical properties of micro-alloyed MgZnCa and MgZnGe alloys", *Mater. Des.*, vol. 185, p. 108285, jan. 2020, doi: 10.1016/j.matdes.2019.108285.

P.-R. Cha *et al.*, "Biodegradability engineering of biodegradable Mg alloys: Tailoring the electrochemical properties and microstructure of constituent phases", *Sci. Rep.*, vol. 3, n° 1, p. 2367, dez. 2013, doi: 10.1038/srep02367.

R. Hou *et al.*, "In vitro evaluation of the ZX11 magnesium alloy as potential bone plate: Degradability and mechanical integrity", *Acta Biomater.*, vol. 97, p. 608–622, out. 2019, doi: 10.1016/j.actbio.2019.07.053.

S. A. Abdel-Gawad e M. A. Shoeib, "Corrosion studies and microstructure of Mg−Zn−Ca alloys for biomedical applications", *Surf. Interfaces*, vol. 14, p. 108–116, mar. 2019, doi: 10.1016/j.surfin.2018.11.011.

S. Cai, T. Lei, N. Li, e F. Feng, "Effects of Zn on microstructure, mechanical properties and corrosion behavior of Mg–Zn alloys", *Mater. Sci. Eng. C*, vol. 32, n° 8, p. 2570–2577, dez. 2012, doi: 10.1016/j.msec.2012.07.042.

S. E. Harandi, M. Mirshahi, S. Koleini, M. H. Idris, H. Jafari, e M. R. A. Kadir, "Effect of calcium content on the microstructure, hardness and in-vitro corrosion behavior of biodegradable Mg-Ca binary alloy", *Mater. Res.*, vol. 16, n° 1, p. 11–18, nov. 2012, doi: 10.1590/S1516-14392012005000151.

S. Virtanen, "Biodegradable Mg Alloys: Corrosion, Surface Modification, and Biocompatibility", in *Biomedical Applications*, vol. 55, S. S. Djokić, Org. Boston, MA: Springer US, 2012, p. 101–125.

T. Kokubo e H. Takadama, "How useful is SBF in predicting in vivo bone bioactivity?", *Biomaterials*, vol. 27, n° 15, p. 2907–2915, may 2006, doi: 10.1016/j.biomaterials.2006.01.017.

W. Du, K. Liu, K. Ma, Z. Wang, e S. Li, "Effects of trace Ca/Sn addition on corrosion behaviors of biodegradable Mg–4Zn–0.2Mn alloy", *J. Magnes. Alloys*, vol. 6, n° 1, p. 1–14, mar. 2018, doi: 10.1016/j.jma.2018.01.004.

Y. Gao *et al.*, "Effect of stress on corrosion of high-purity magnesium in vitro and in vivo", *Acta Biomater.*, vol. 83, p. 477–486, jan. 2019, doi: 10.1016/j.actbio.2018.11.019.

Y. Lu, A. Bradshaw, Y. L. Chiu, e I. Jones, "Investigation of the Microstructure and Bio-Corrosion Behaviour of Mg-Zn and Mg-Zn-Ca Alloys", *Mater. Sci. Forum*, vol. 765, p. 788–792, jul. 2013, doi: 10.4028/www.scientific.net/MSF.765.788.

Y. Song, E.-H. Han, D. Shan, C. D. Yim, e B. S. You, "The effect of Zn concentration on the corrosion behavior of Mg–xZn alloys", *Corros. Sci.*, vol. 65, p. 322–330, dez. 2012, doi: 10.1016/j.corsci.2012.08.037.

Z. Shi e A. Atrens, "An innovative specimen configuration for the study of Mg corrosion", *Corros. Sci.*, vol. 53, n° 1, p. 226–246, jan. 2011, doi: 10.1016/j.corsci.2010.09.016.

****